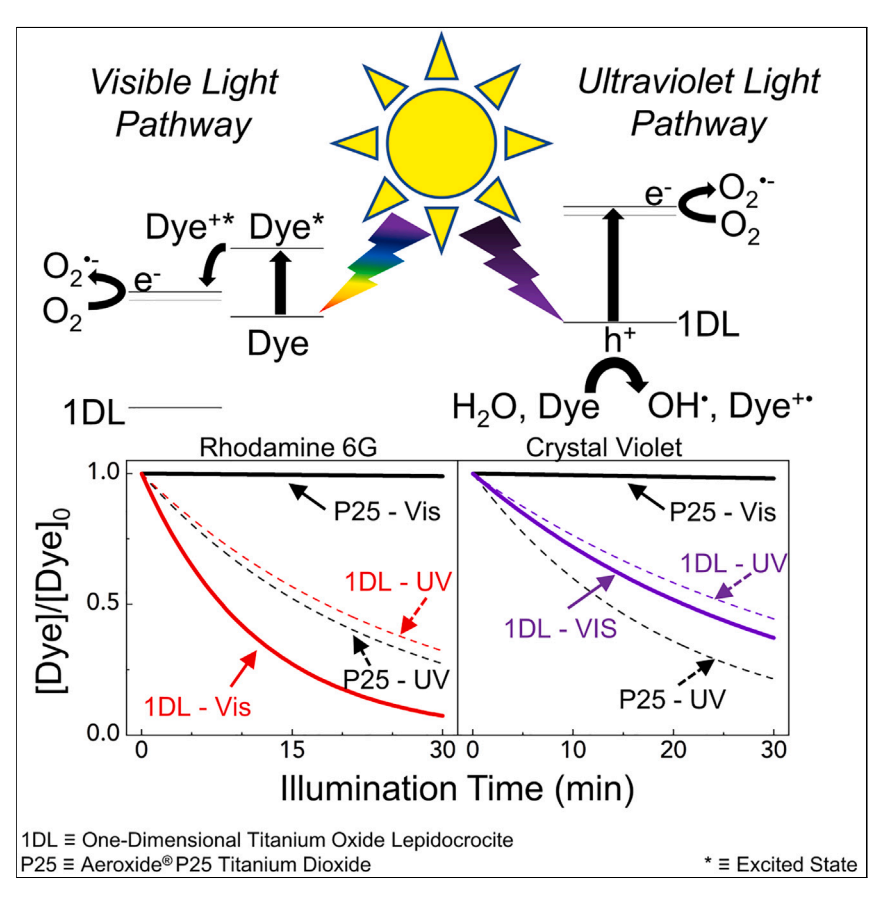
Matter



Article

Adsorption and self-sensitized, visible-light photodegradation of rhodamine 6G and crystal violet by one-dimensional lepidocrocite titanium oxide



Here, we use a colloidal one-dimensional titanium oxide-based photocatalyst to adsorb and degrade the model dyes rhodamine 6G and crystal violet. The high adsorption capacity of the material enables it to degrade the dyes via self-sensitization, requiring light from only the visible range. We characterize and discuss the properties of these one-dimensional photocatalysts and demonstrate their applicability in water treatment applications.

Adam D. Walter, Gregory R. Schwenk, Jacob Cope, ..., Andrea Mininni, Andrew J. Lindsay, Michel W. Barsoum

barsoumw@drexel.edu

Highlights

One-dimensional titanium oxidebased material with 5 \times 7 \mathring{A}^2 cross section

High adsorption capacity of cationic dyes primarily due to ion exchange

Self-sensitized decolorization of dyes occurs under visible light irradiation

Photocatalytic activity elicits mineralization of dyes to gaseous substances



Demonstrate

Proof-of-concept of performance with intended application/response

Walter et al., Matter 6, 4086–4105 November 1, 2023 © 2023 Elsevier Inc. https://doi.org/10.1016/j.matt.2023.09.008







Article

Adsorption and self-sensitized, visible-light photodegradation of rhodamine 6G and crystal violet by one-dimensional lepidocrocite titanium oxide

Adam D. Walter,¹ Gregory R. Schwenk,¹ Jacob Cope,¹ Kaustubh Sudhakar,¹ Mary Qin Hassig,¹ Lucas Ferrer,¹ Andrea Mininni,¹ Andrew J. Lindsay,² and Michel W. Barsoum^{1,3,*}

SUMMARY

A one-dimensional (1D) lepidocrocite structured titanium oxide photocatalyst, in which the cross-sections of the base unit are $\approx 5\times 7~\text{Å}^2$, was evaluated for its ability to decolorize and degrade two common dye pollutants, rhodamine 6G (Rh6G) and crystal violet (CV), under a full simulated solar spectrum as well as UV and visible light spectra seperately. The materials were characterized by X-ray diffraction as well as scanning and transmission electron microscopy. The dye decolorization was monitored via UV-visible spectroscopy. Mineralization was quantified by chemical oxygen demand. As a colloidal nanomaterial, the 1D material presents exceptional maximum uptake for Rh6G and CV at 1,850 mmol kg $^{-1}$ and 1,930 mmol kg $^{-1}$, respectively. They also become dye sensitized and can decolorize Rh6G and CV using visible light only, by an average of 90% and 64%, respectively, in 30 min when the starting catalyst-to-dye mass ratio is 1:1.

INTRODUCTION

Leftover dyes in wastewater represent a major environmental problem. Toxic and persistent cationic dyes have many applications in industry. For example, crystal violet (CV), a triphenylmethane dye, is used to dye ink and textiles, ¹ and rhodamine 6G (Rh6G), a xanthene-derived dye, is used in wood processing and paper dyeing as well as in pen ink and cosmetics. ² The industrial use of water-soluble dyes produces high quantities of toxic and potentially cancer-causing wastewater. ^{3,4} Common wastewater treatment methods—like sedimentation, biological oxidation, and chemical-physical treatment—are generally unsuccessful with dyes because of the complex chemistries often presented by the aromatic systems of such molecules. ³ Alternatively, adsorption is a common method of dye removal with clay materials, ^{5,6} activated carbon, ⁷ iron oxide, ⁸ and natural materials such as coffee grounds. ⁹ Clays—especially montmorillonite—exhibit high cationic dye uptake because of their capability to exchange the dye with their interlayer ionic stabilizers. ⁶ Although these show promise, they simply allow separation of the dye from solution; the dye still exists but is now attached to the adsorbent. Said otherwise, the problem remains.

Rather than separation via adsorption, an attractive method to eliminate dyes from wastewater is to use photocatalysts to break them down into simple compounds such as water, carbon dioxide, and nitrogenous species. The use of Rh6G and CV in industrial and medical applications make such dyes a strong model for photocatalyst activity studies. Common photocatalysts, comprised of titanium dioxide (TiO_2) or titania, are available as anatase, rutile, and amorphous structures. Aeroxide

PROGRESS AND POTENTIAL

Semiconducting photocatalysts are at the forefront of water treatment applications because of their stability, non-toxicity, and low cost. As the dimensions of a material decrease, its specific surface area and activity increase. Here, we report on a onedimensional lepidocrocite, titanium oxide-based colloidal nanomaterial for water treatment. The material adsorbs large amounts of rhodamine 6G and crystal violet textile dyes, partially because of record-high surface areas and favorable surface interactions. These dyes also sensitize the material, allowing it to degrade the dyes using visible light only, despite a wide bandgap energy of ≈ 4 eV. This sensitization offers significant potential for the material in a multitude of applications such as photocatalysis, water treatment, and optoelectronic devices, among many others.





P25, hereafter referred to as P25 (made by Evonik, formerly made by Degussa) contains a blend of all three $^{13-15}$ and is used as a standard in many studies on $\rm TiO_2$ photocatalysts. $^{16-21}$ The illumination of a semiconductor photocatalyst like $\rm TiO_2$ in an aqueous system results in the formation of electron-hole pairs that, in turn, produce reactive oxygen species (ROS). The resulting ROS, along with the holes themselves, oxidize the polluting dye into smaller fragments. $^{22-24}$

The key to dye degradation is the ability of a photocatalyst to generate electron holes and ROS: hydroxyl radical ('OH), superoxide (O_2 '–), and singlet oxygen (1O_2). Holes—or localized missing electrons—are the strongest oxidizing species. Semiconductors form holes in their valence band (VB) by absorbing light with an energy that is greater than their optical band-gap energy (E_g), which promotes an electron to the conduction band (CB). The photogenerated holes may oxidize surface hydroxyl terminations and adsorbed water to produce 'OH radicals as a part of indirect oxidation—with respect to direct oxidation by the holes themselves—and only play a role with weakly adsorbed molecules. The degradation mechanism of the waste dyes is generally attributed to the presence of both holes and 'OH.3

Because TiO_2 -based photocatalysts have an E_g wider than 3.0 electron volts (eV) they generally lack visible light activity. To solve this problem, dye sensitization is a method to improve their overall spectral usage. Unlike most heterogeneous photocatalyst systems, where the photon directly excites an electron from the VB of a semiconductor into its CB, $^{16,24-26}$ sensitization enables electron transfer from the excited state of the dye into the CB of the semiconductor. $^{10,18,27-31}$ Dye sensitization is a common method used in solar cell applications to improve visible light absorbance. 29 However, in aqueous systems, the dye can actually aid the photocatalyst in its ultimate self-demise. This phenomenon is called self-sensitization, and its occurrence with TiO_2 nanoparticles has been studied in dye-containing aqueous solutions, such as rhodamine B^{32} and eosin. 33 These mechanisms rely on forming O_2 , which, in turn, forms the remaining ROS through reactions with water. Self-sensitization processes remove the need for narrow-band-gap semiconductors. Instead, electrons in the dye's excited state, stimulated by visible light, can access the CB of the semiconductor and react with dissolved oxygen to yield ROS. 32,33

For self-sensitization to occur, a certain synergy must be established between the dye and semiconductor. From the semiconductor perspective, a wide E_g, high CB energy, large specific surface area, and affinity for the sensitizing dye are preferred.^{29,32,33} It is imperative for the excited state of the dye molecule to exist at a higher energy than the CB of the semiconductor; therefore, this excited state provides direct access to the CB, effectively bypassing the need to excite the semiconductor.³² Second to band alignment, adsorption is key to sensitization. The contact between the dye and photocatalyst must allow efficient electron transfer and, ultimately, ROS generation. There is also work that concludes that a hydrated surface with accessible bridging oxygen (Ti-O-Ti) surface sites for electrostatic interactions with the dyes is integral for improved electron transfer.^{27,31}

In general, one-dimensional (1D) titanium oxide-based nanomaterials (i.e., nanotubes, nanowires, etc.) are synthesized by high temperature, high pressure, or complex methods such as the hydrothermal, solvothermal, chemical vapor deposition, and templating methods, among others. ^{34–36} In addition to difficult syntheses, the current undoped or non-composited 1D TiO₂ photocatalysts suffer from fast electron-hole recombination rates and low specific surface areas. ^{36,37} Finding a material that overcomes these hurdles would open the door to extensive improvements in a

¹Department of Materials Science and Engineering, Drexel University, 3141 Chestnut St., Philadelphia, PA 19104, USA

²Department of Chemistry, Drexel University, 3201 Chestnut St., Philadelphia, PA 19104, USA

Blood contact

^{*}Correspondence: barsoumw@drexel.edu https://doi.org/10.1016/j.matt.2023.09.008





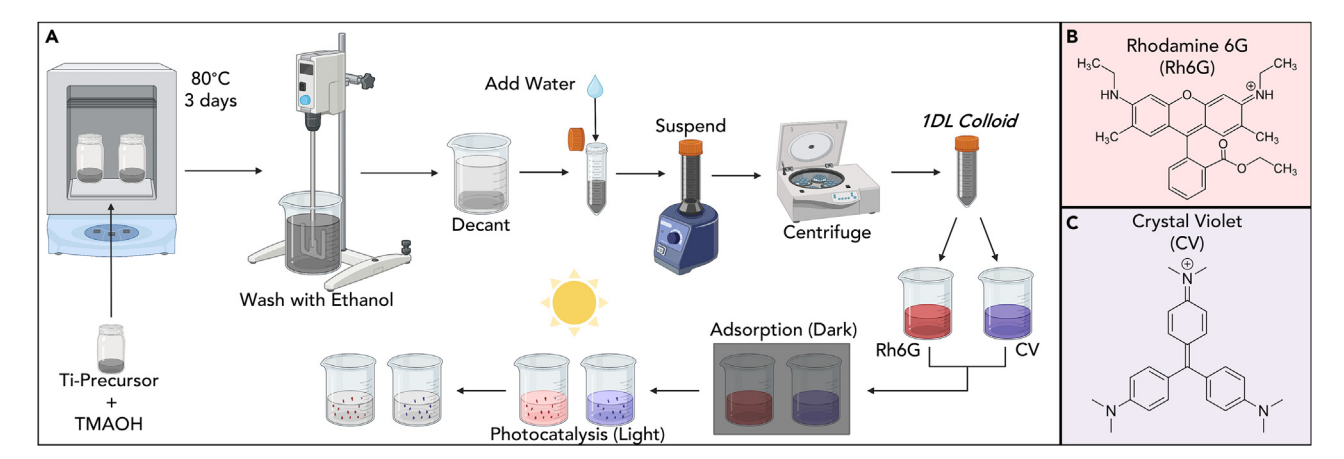


Figure 1. Schematic of the study demonstrating synthesis and photocatalytic degradation of dyes by 1DLs

(A) Diagram detailing the synthesis of 1DLs in their colloidal form. Colloidal 1DLs are added to the dye solutions and left in the dark for 30 min to establish adsorption equilibrium, after which they are exposed to light to degrade the dye.

(B and C) Chemical structures of (B) Rh6G and (C) CV.

wide array of applications from pollutant degradation, discussed here, to solar cells and chemical production. 36,37

We recently discovered that, when more than a dozen water-insoluble, non-toxic, earth-abundant, Ti-containing compounds are submerged in 25% (w/w) tetramethy-lammonium hydroxide (TMAOH) aqueous solutions they transform, after a few days of mixing, at ambient pressure and temperatures less than 100°C, into veritable 1D lepidocrocite titanium oxide-based nanofilaments, hereafter referred to as 1DLs. ^{38,39} As outlined in Figure 1A, the process to synthesize 1DLs is facile, requiring no specialized equipment, and scalable. 1DLs form extremely stable aqueous colloids, a property that is leveraged to separate product from precursor material. ^{38,39} With some precursors, like titanium diboride (TiB₂), the precursor mostly used in this study, near-full conversion can be obtained, furthering the appeal of the production process.

In contrast to previous work in the literature discussing 1D titanium oxide materials, 1DLs, as far as we are aware, are the only ones where, at $\approx 5 \times 7$ Ų, the minimal cross-section is in the sub-nanometer scale. Nano-bundles of 1DL are visible by scanning transmission electron microscopy, shown in our more detailed work on characterization. ^{38,39} Using the minimal cross-section as a base unit, the theoretical specific surface area is estimated to be around 1,000 m²/g, and that is assuming only two sides of the 1DL are available for adsorption. One of the attractive attributes of 1DLs, germane to this study, is the ease by which cationic exchange can occur. Exchange has been demonstrated with an array of cations, including a variety of group I and II cations ⁴⁰ and actinides. ⁴¹

At the X-ray diffraction (XRD), X-ray photoelectron spectroscopies (XPS), and Raman spectroscopy levels, all 1DLs appear to be quite similar, independent of precursor chemistry. 38,39 With respect to optical properties, 1DLs have an indirect E_g of ≈ 4 eV, also irrespective of precursor chemistry. 38,42 Note that this E_g is significantly larger than that of anatase nanoparticles, at ≈ 3.2 eV, or 2D nanosheets, at 3.6 eV, 43 a feature that we attribute to quantum confinement to one dimension. 1DLs also exhibit long photoexcitation lifetimes, in the realm of nanoseconds. 42

The purpose of this work is to demonstrate, for the first time, the use of unmodified colloidal 1DLs as a flocculating adsorbent and photocatalytic material for the



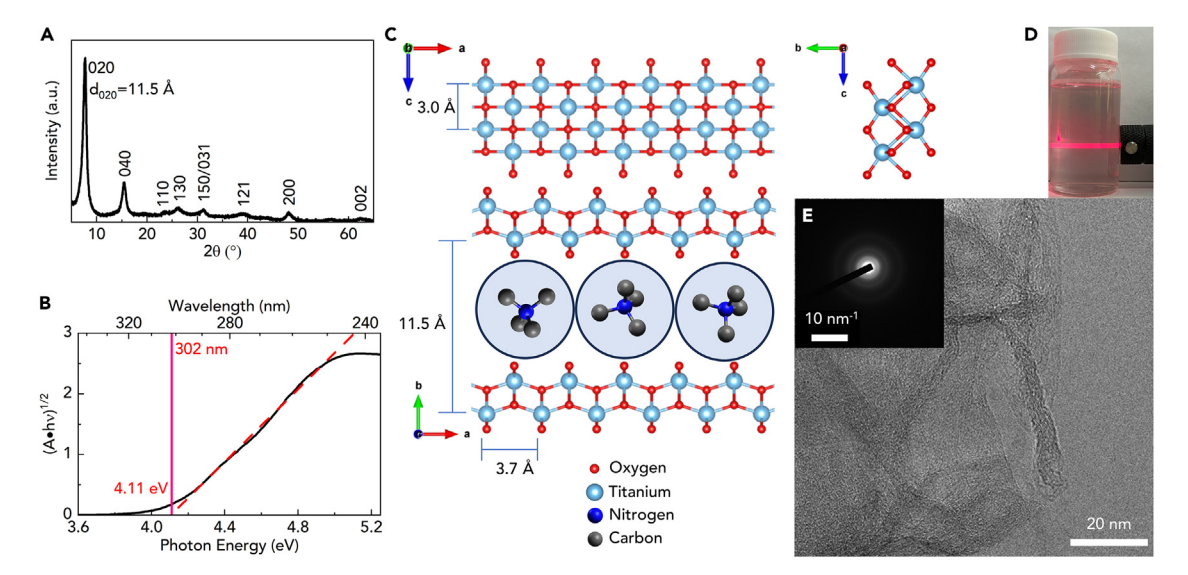


Figure 2. Structural and optical properties of 1DLs

- (A) XRD pattern of filtered 1DL colloid crushed into a fine powder.
- (B) Tauc plot showing indirect band gap of 1DL colloid at a concentration of 10 mg/L.
- (C) DFT-predicted 1DL structure, including d₀₂₀, with the a and c parameters. Cross-section shown at top right is a minimal cross-section.
- (D) Tyndall effect exhibited in colloidal 1DL diluted to 1 g/L.
- (E) TEM micrograph showing drop-cast 1DL onto a lacy carbon grid. Inset: associated SAED pattern.

degradation of Rh6G and CV. We characterize the flocculated material and demonstrate that self-sensitization is the primary driver for its photocatalytic activity, best seen by dye decolorization under visible light only.

RESULTS

1DL structure and optical properties

The XRD pattern of the sample used primarily in this study, on a linear scale (Figure 2A), matches that of the patterns reported in our earlier work. ³⁹ XRD peak assignments, and associated d-spacings, are listed in Table S1. It is important to note here that, in our earlier work, we incorrectly assigned the low angle peak to (00I). More recent work, however, has shown them to be (0k0) peaks (where k is a multiple of 2), as shown here. This low-angle peak and its reflections correspond to the center-to-center distance between two adjacent 1DLs. In other words, they self-assemble, or stack, in the *b* direction in an ABA manner.

This d-spacing shifts depending on the nature of the cations between the 1DLs. ⁴⁰ When the interplanar spacing is filled with tetramethylammonium cations (TMA⁺), resulting from the synthesis procedure, the peak is present at $2\theta \approx 7.7^{\circ}$, corresponding to $d_{020} \approx 11.5$ Å, as shown in Figure 2A. The (200) peak at $2\theta \approx 48^{\circ}$ is not processing dependent and is the distance between Ti layers along the a growth direction of the 1DLs. Additionally, the (002) peak at $2\theta \approx 62^{\circ}$ is the distance between Ti atoms in the lattice perpendicular to the growth direction, viz. c direction. The a and c lattice parameters obtained from these peaks, 3.0 Å and 3.7 Å, respectively, agree well with those of lepidocrocite ⁴⁴ despite the fact that it is *two-dimensional* (2D), while here we are dealing with its 1D counterpart. A to-scale structure of a 1DL predicted using density functional theory (DFT) is shown in Figure 2C, showing the a and c parameters, along with d₀₂₀, from the XRD in Figure 2A. Note that the cross-section shown in Figure 2C is a minimal cross-section.





The Tauc plot of colloidal 1DLs, generated from the liquid-phase light absorbance of a colloid diluted to 10 mg/L, is illustrated in Figure 2B. This result closely follows that of a recent work by Colin-Ulloa et al. 42 who generated Tauc plots from thin films in transmission. Figure 2D shows the Tyndall effect in the suspension diluted to a concentration of 1 g/L, indicative of a colloidal material.

Transmission electron microscopy (TEM) micrographs, like the one in Figure 2E, show that, when dried, the 1DLs bundle and form pseudo-2D flakes. Many of the 2D flakes, however, are amorphous, as indicated by the lack of sharp rings in the selected area electron diffraction (SAED) pattern in the top inset in Figure 2E. Ongoing work is looking into the mechanisms of self-assembly. Directly imaging the 1DLs in colloidal form has proven to be difficult, and we are still working to obtain in situ micrographs of the colloidal material. In an effort to image them in a confocal microscope, a fluorescence dye (Rh6G) was added to the colloidal 1DLs. The colloidal suspension formed coagulated particles that did not allow us to image individual 1DLs; however, this coagulation spawned nearly this entire study.

Adsorption of Rh6G and CV onto 1DL

Room-temperature adsorption kinetics and isotherm data were obtained at a neutral pH for Rh6G and CV on colloidal 1DLs. The kinetic data were fit to Lagergren's pseudo-first order (PFO) and Ho's pseudo-second-order (PSO) adsorption rate laws in their respective non-linear forms. The PFO and PSO rate laws can be described by $q = q_{\rm eq}(1 - {\rm e}^{-k_1 t})$ and $q = \frac{q_{\rm eq}^2 k_2 t}{1 + q_{\rm eq} k_2 t}$, respectively, where q is uptake at time t, $q_{\rm eq}$ is equilibrium uptake, and k_1 and k_2 are the PFO and PSO rate constants, respectively. The isotherm data were fit to the modified Langmuir and Freundlich isotherm equations. The modified Langmuir equation used in this study is as follows: $q_{\rm eq} = q_{\rm max} \frac{k_L C_{\rm eq}}{1 + k_L C_{\rm eq}}$, where $q_{\rm eq}$ is equilibrium uptake, $q_{\rm max}$ is maximum uptake, k_L is the Langmuir constant, and $C_{\rm eq}$ is the equilibrium concentration. Last, the Freundlich isotherm equation used is $q_{\rm eq} = k_F C_{\rm eq} \frac{1}{n}$, where $q_{\rm eq}$ is equilibrium uptake, k_E is the Freundlich constant, $C_{\rm eq}$ is equilibrium concentration, and n is a constant of linearity.

Both PFO and PSO rate laws fit the data well, as illustrated in Figure 3, but for Rh6G and CV, the PFO rate law resulted in better fits. The adsorption behavior follows a

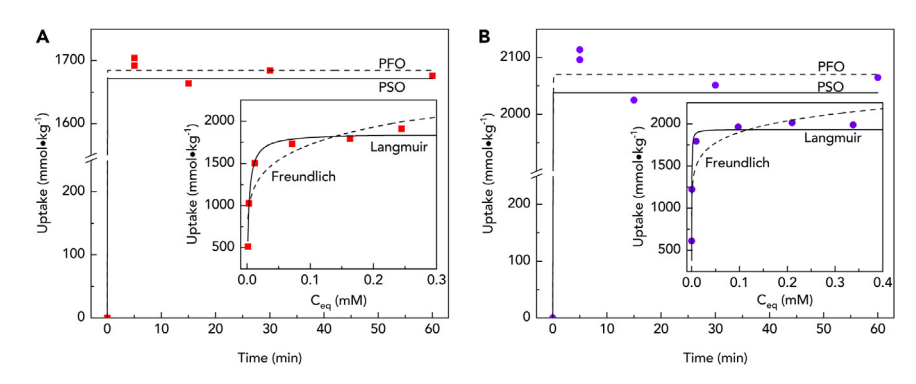


Figure 3. Room-temperature adsorption characteristics for Rh6G and CV on 1DL Adsorption of (A) Rh6G (red squares) and (B) CV (purple circles) on 1DL. Outer plots indicate the kinetics data fit to the PFO (dashed) and PSO (solid) rate laws as indicated. Insets: equilibrium plots with fits to the Langmuir (solid) and Freundlich (dashed) isotherm relations. Fitting results are listed for the kinetic and isotherm data in Tables S2 and S3, respectively.



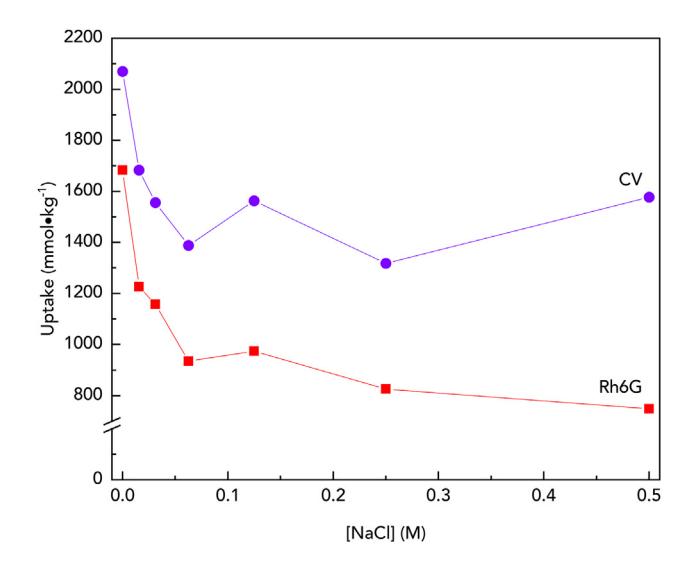


Figure 4. Maximum uptake for Rh6G and CV on 1DL as a function of NaCl concentration Rh6G, red squares; CV, purple circles.

step-like function on the current timescale. It appears that the adsorption capacity of the colloidal 1DL is filled near-instantaneously. With regard to the isotherm data, the modified Langmuir model fits the data for both dyes better than the Freundlich model. The maximum uptake values for Rh6G and CV are 1,850 mmol $\rm kg^{-1}$ and 1,930 mmol $\rm kg^{-1}$, respectively. The CV adsorption, shown in Figure 3B, inset, shows a more dramatic inflection than that of the adsorption of Rh6G (Figure 3A, inset). The fitting parameters for the kinetic and isotherm plots shown in Figure 3 are listed in Tables S2 and S3, respectively.

Introducing a competitive cation, such as Na^+ , reduces the equilibrium uptake for both dyes on 1DL, as shown in Figure 4. 1DLs lose \sim 38% of uptake capacity for CV and \sim 52% for Rh6G.

Complexation and flocculation

In an effort to compare our work with existing literature, 11,22,45 early experiments were conducted with high catalyst-to-dye mass ratios—upward of 100:1. At these ratios, we observed an immediate color change, but the suspension remained homogeneous. However, in an effort to reasonably conserve material, we settled on an initial trial of a 10:1 catalyst-to-dye ratio. Note that, in this experiment, the dye concentration was 10 mg/L. After 30 min of stirring in the dark, the intensity of the absorbance at the wavelength of maximum absorbance (λ_{max}) is reduced, and a hypsochromic peak shift occurs (red line in Figure 5A). Interestingly, the colloidal suspension, as shown by the Tyndall effect in Figure S2, is maintained. When exposed to light, there is an immediate color change (Figure 5C), accompanied by a bathochromic shift, peak broadening, and overall intensity decrease (Figure 5A). If the system is filtered through Celgard to remove the 1DLs, it becomes apparent that essentially all of the dye is adsorbed (Figure 5B).

At 1DL-to-dye mass ratios closer to 1:1, after about 10 s, large, colored flocs, visible to the naked eye, appear that are easily removable via filtration. For the ratio used in the majority of this study (1:1 1DL-to-dye by mass), adsorption remains significant, and colored flocs are present (Figures 6A and 6C). Importantly, irradiating the





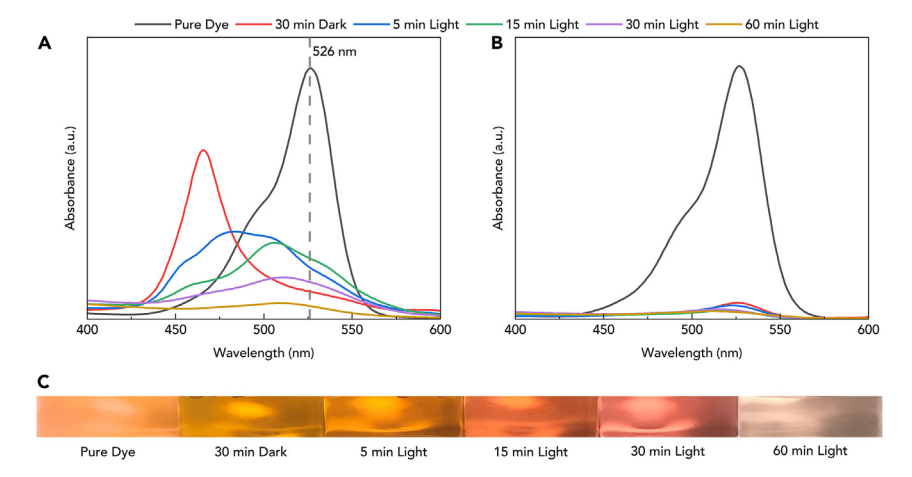


Figure 5. Time dependencies of UV-vis scans for 10:1 mass ratio 1DL to Rh6G for an illuminated run

(A and B) Unfiltered (A) and filtered (B) to remove the complex.
(C) Color change in the unfiltered complex with increasing illumination times. Starting dye concentration was 10 mg/L.

mixture for 60 min resulted in solution decolorization and a concomitant reduction in overall floc size (Figures 6B and 6D). The scanning electron microscope (SEM) micrograph shown in Figure 6E illustrates how the 1DLs assemble into 2D sheets that, in turn, aggregate into microscale particles. The inset in Figure 6E captures the "bundling" of the individual 1DLs into sub-micrometer-thick fibers. Note the fine features observed for these flocs, further evidences the 1D nature of these materials.

The XRD patterns for water-washed and dried Rh6G/1DL and CV/1DL flocs are shown in Figure 6F. The same results, plotted as semi-log plots, are shown in insets in same and evidence a d-spacing shift between each 1DL with the introduction of the dye. Note that the non-processing-dependent peaks for (200) at $2\theta \approx 48^\circ$ and (002) at $2\theta \approx 62^\circ$ are still present, indicating that the structure of the individual 1DL is maintained. There is a noticeable difference between relative peak intensities between the (020) and (200) peaks—at $2\theta \approx 7.5^\circ$ and $\approx 48^\circ$, respectively between the CV and Rh6G patterns in Figure 6F. This indicates that the stacking in the *b* direction occurs more readily in the Rh6G flocs than their CV counterparts.

1DL photocatalytic behavior

Because of the high adsorption capacity of the 1DLs, the starting concentrations drop from 10 mg/L of dye to around 4 mg/L of dye during the first 30 min in the dark, as shown in Figure S3. P25, on the other hand, adsorbs significantly less dye on a similar timescale, so at least 9 mg/L of dye remains in solution. As a result, the total dye removal, as shown in Figure S3, greatly favors 1DLs over P25. In terms of 1DL precursors, 1DL and N-1DL, derived from TiB₂ and titanium nitride (TiN), respectively, behave essentially the same in removing Rh6G from water, while C-1DL, derived from titanium carbide (TiC), adsorbed much less than its counterparts but performed similarly as a photocatalyst (Figure S3A).

When comparing photocatalytic activity, alone, the concentrations were normalized by the concentrations present, after adsorption in the dark, and the resulting PFO kinetic parameters were obtained. The PFO rate law can be described by $[Dye]/[Dye]_0 = 1 - e^{-k_1t}$; where [Dye] is the concentration at time t, $[Dye]_0$ is the

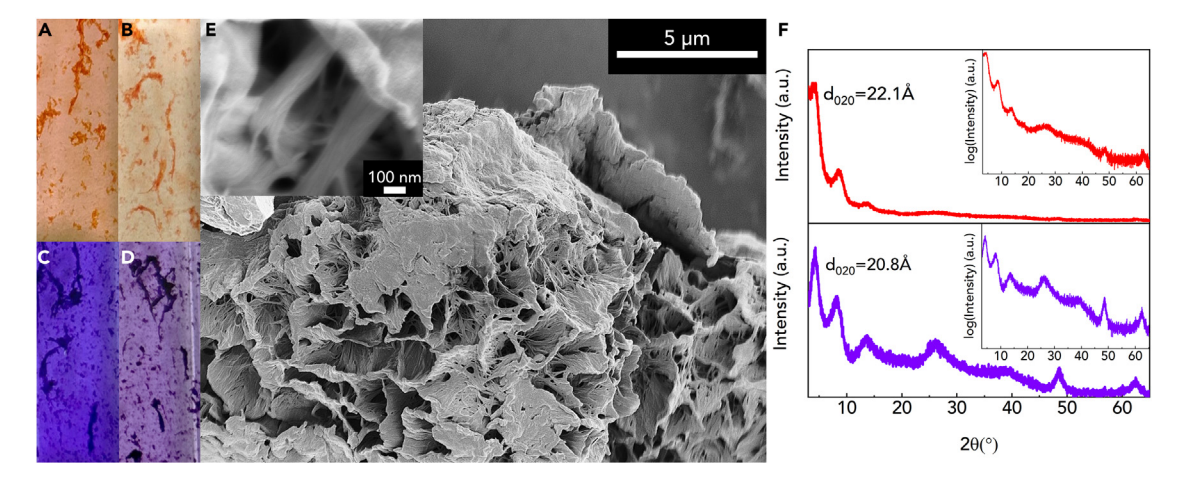


Figure 6. Characterization of flocs

(A and B) Photo before (A) and after (B) illumination of 1DL/Rh6G flocs.

(C and D) Photo before (C) and after (D) illumination of 1DL/CV flocs.

(E) SEM micrograph of 1DL/Rh6G floc freeze dried in liquid nitrogen. Top inset: a high-magnification SEM micrograph illustrating the fibrous nature of the 1DLs.

(F) XRD patterns of dried flocs for 1DL/Rh6G (top) and 1DL/CV (bottom). Insets: semi-log plots for each pattern.

initial concentration after reaching adsorption equilibrium, and k_1 is the PFO constant. As shown in Figure 7A, the 1DLs outperform P25 significantly in decolorizing Rh6G, with rate constants of 0.12 min⁻¹ and 3.1 × 10^{-2} min⁻¹, respectively. For CV, shown in Figure 7B, the situation is different in that 1DLs and P25 performed equally well with a rate constant of $\approx 3.1 \times 10^{-2}$ min⁻¹ each.

The solid and dashed black lines, with right-hand y axis and hollow data points, in Figures 7A and 7B illustrate the hypsochromic shift with irradiance time, consistent with the formation of n-dealkylated intermediates related to the degradation mechanisms of each dye. ^{3,30,46} These shifts are an additional method of tracking the dealkylation and overall dye degradation rather than decolorization alone. When no degradation occurs, as in the case of adsorption (unless there is complexation, as outlined in Figure 5A), the wavelength of maximum absorption of the solution does not shift.

When illuminated by UV light only, applying a filter to block visible light, the dyes decolorize over both catalysts (dashed lines, Figures 7C and 7D), as expected. With PFO kinetic rate constants of $3.8 \times 10^{-2} \, \mathrm{min^{-1}}$ and $4.3 \times 10^{-2} \, \mathrm{min^{-1}}$, respectively, the UV activity of the 1DLs is comparable with P25 for Rh6G (dashed lines, Figure 7C). In contrast, at $5.1 \times 10^{-2} \, \mathrm{min^{-1}}$ and $2.7 \times 10^{-2} \, \mathrm{min^{-1}}$, respectively, the rate constant of P25 is roughly double that of 1DLs for decolorization of CV under UV light (dashed lines, Figure 7D). Indeed, we measure *significant* dye decolorization using the 1DLs (solid colored lines, Figures 7C and 7D) even when *only the visible spectrum* is used. Under these conditions, P25 is essentially inactive on this timescale (solid black lines, Figures 7C and 7D). This result is the most important of this work. As discussed below, it implies that the dyes sensitize the 1DLs.

Confirmation of dye mineralization via COD

Chemical oxygen demand (COD) is a wastewater analysis technique in which all compounds containing hydrogen, carbon, oxygen, and nitrogen are oxidized to their





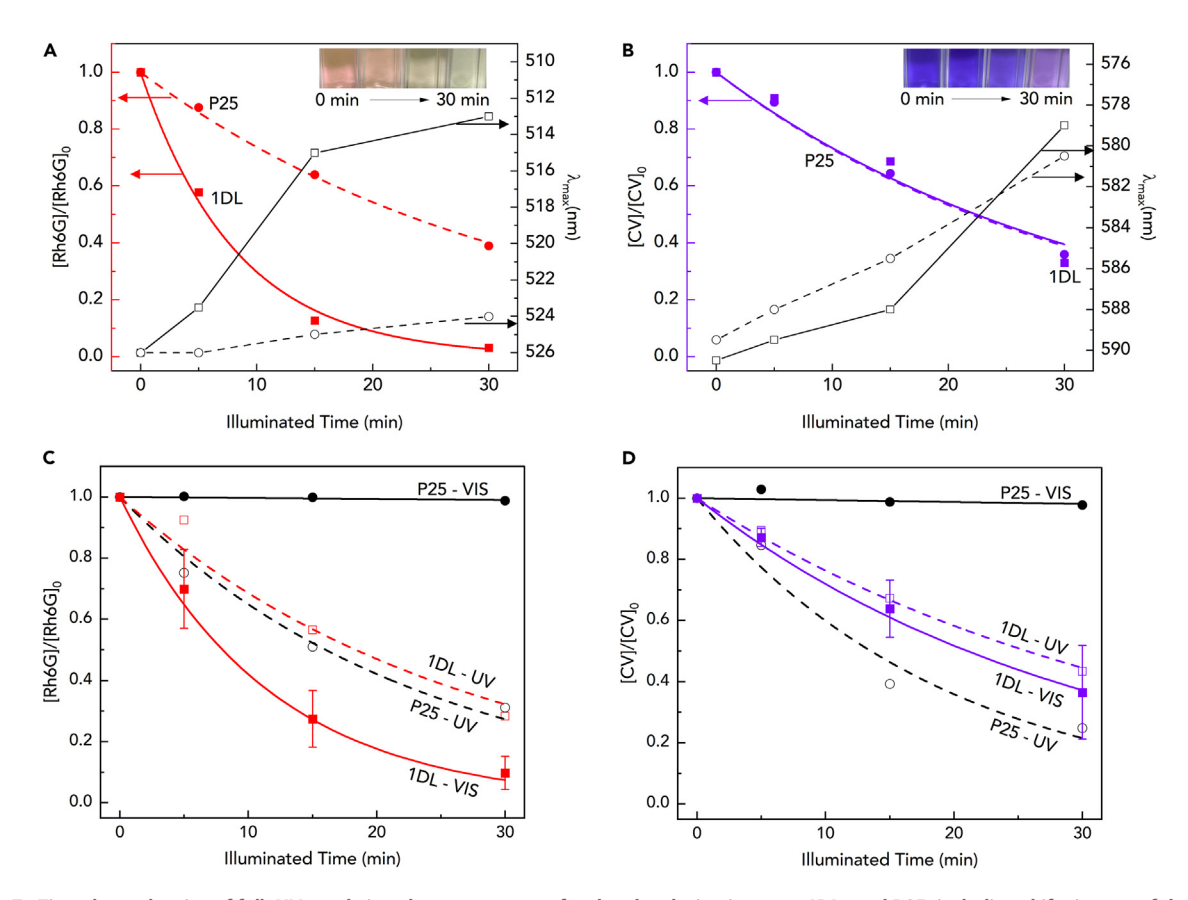


Figure 7. Time dependencies of full, UV-, and vis-only spectrum runs for dye decolorization over 1DLs and P25, including shifts in λ_{max} of dyes over 1DLs and P25 under a full spectrum

Time dependence of decolorization (left axis) for (A) Rh6G over 1DLs (red squares) and P25 (red circles) and (B) CV over 1DLs (purple squares) and P25 (purple circles). PFO fits for 1DL (solid, colored) and P25 (dashed, colored). Readings were taken at 526-nm and 590-nm wavelengths for Rh6G and CV, respectively. Time dependencies of hypsochromic shifts (right axis) in λ_{max} for 1DLs (solid, black) and P25 (dashed, black). Insets: color change throughout the dye removal process. Also shown is decolorization of (C) Rh6G, and (D) CV over 1DL and P25. Solid lines denote activity with visible light only. Dashed lines denote activity with UV light only. Data points correspond to the average of 3 runs. Error bars correspond to one standard deviation between runs. Note that P25 is totally inactive in the visible range. PFO fits are plotted as lines in the same color as the latter. Dyes were in a 1:1 mass ratio to 1DLs; starting dye concentration was 10 mg/L. Transient concentrations are normalized by concentration after 30 min in the dark, [Rh6G]₀ and [CV]₀. Fitting parameters and statistics are listed in Tables S4 and S5 for (A) and (B) and (C) and (D), respectively.

fullest extent by dichromate ions under acidic conditions (generally sulfuric acid). It allows direct comparison of the concentration of organic matter between two water samples. As seen in Figure 8, there is a greater than 50% reduction in COD for Rh6G and CV in 60 min. Additionally, it is evident that Rh6G is decolorized easier than CV, but the COD reduction is quite similar between the two, with reductions of 52% and 60%, respectively. The kinetics of COD reduction have PFO rate constants of 1.1 x 10^{-2} min⁻¹ and 1.6 x 10^{-2} min⁻¹ for Rh6G and CV, respectively. Table S6 outlines the fitting parameters for both (Figure 8).

In addition to COD, we completed an introductory liquid chromatography-mass spectrometry (LC-MS) study to ensure degradation of Rh6G over illuminated 1DL. An abridged version of the LC-MS data is available in Figure S6, detailing the change between the pure dye Rh6G after 60 min of illumination. The importance of this figure relies on the peak reduction of the peak at an elution time of 8.78 min between Figures S6A and S6B. This peak corresponds to the Rh6G molecule, indicating that



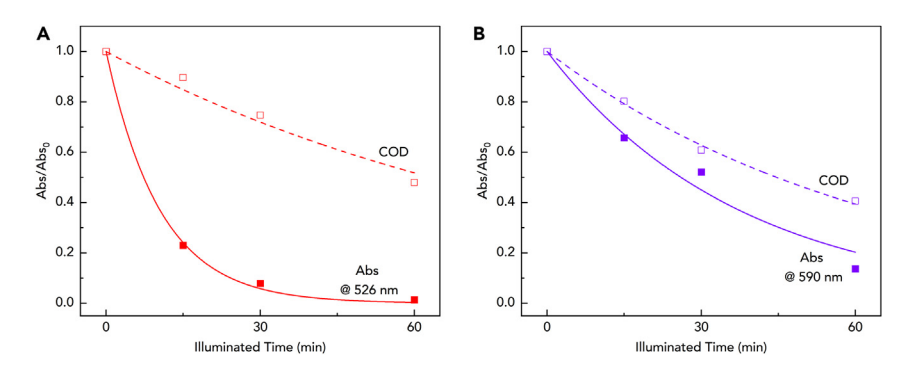


Figure 8. Comparison between absorbance and COD methods of quantifying dye mineralization Decolorization and COD of, (A) Rh6G, and (B) CV over 1DLs under full-spectrum irradiance. Dyes were in a 1:1 mass ratio to 1DL; starting dye concentration was 50 mg/L. Lines through the data points are PFO fits for each dataset; fitting parameters are listed in Table S6.

after 60 min the majority signal from the pure dye is missing. A full mechanistic study of the degradation of dyes used here is outside the scope of this work.

DISCUSSION

The information outlined in Table 1 illustrates the high adsorption capacity exhibited by colloidal 1DLs in adsorbing Rh6G and CV. Because the adsorption capacity of colloidal 1DLs was so high, we carried out a comparative study with montmorillonite (MMT) clay to ensure that our measurements were accurate (Figure S1). This was indeed the case because we found MMT adsorption behavior similar to that published in the literature (Table 1). MMT clay was chosen for comparison because of its technological maturity. P25 is not included here because its ability to take up dye molecules is significantly lower than the materials included in Table 1. The adsorption of activated carbon is also listed in Table 1. A perusal of all of these values indicates that the adsorption by 1DLs is significantly higher than MMT clay or activated carbon.

In terms of our current understanding of 1DL surface chemistry, they are highly hydrophilic and remain as stable colloids for months without separation, indicative of a highly charged surface. At a pH of 7, the zeta potentials of mesoporous particles comprised of 1DLs are in the -50 to -60 mV range. ^{40,41} Upon addition of water to the ethanol-washed product, we see a pH spike that we attribute to the 1DLs behaving as a Brønsted-Lowry base, accepting protons from the surrounding water. It is crucial to note at this junction that after washing 1DLs with ethanol to neutral and then suspending them in water, the negative charges on the 1DL surfaces are balanced by TMA⁺ cations and any protons captured upon suspension of the 1DL in water. The presence of the TMA⁺ cation leads to a large interfacial dipole normal

Rh6G			CV		
Material	q _{max} (mmol/kg)	Source	Material	q _{max} (mmol/kg)	Source
Colloidal 1DL	1,854	this work	colloidal 1DL	1,933	this work
MMT clay	685	this work	MMT clay	800	Guz et al. ⁴⁷
MMT clay	785	Li et al. ⁶	TiO ₂ nanosheets	118	Chen et al. ²¹
Commercial activated carbon	58.5	Abdullah et al. ⁴⁸	commercial activated carbon	860	Sattar ⁴⁹





to the surface of the 1DLs⁴² that presumably aids in the ability of 1DLs to adsorb cationic species.

We have also recently demonstrated that the primary mode of adsorption of cationic species on 1DLs is ion exchange, 40,41 which is apparently integral to the sensitization effects we observe. When we tried to adsorb anionic dyes or negatively charged entities at neutral pH, no ion exchange was observed. Said otherwise, the main drivers for electron transfer are electrostatic rather than, say, covalent linkages. 27,31 This fact is supported in our work because CV does not contain a common linking group for dye sensitization, such as the ester in Rh6G, but adsorbs at a similar extent as Rh6G. CO_2R groups are considered potential linking groups for many sensitizing applications. $^{27,29-31}$ However, we cannot discount the ability of the lone pairs of the methylated nitrogen atoms on the pendant groups of CV to act as electron pair donors and form a linkage to a 1DL surface.

Introducing a counter-cation, like Na⁺, reduces the maximum uptake for Rh6G and CV on 1DL, shown in Figure 4. The NaCl concentration is much greater than that of either dye, and dye uptake reaches a horizontal asymptotic limit. This again demonstrates that ion exchange is the primary mode of adsorption, but there could also be other favorable interactions, such as hydrogen bonding, between each dye and the surface terminations of the 1DLs. Molecular dynamics simulations related to the adsorption modes of the dyes on 1DLs are the subject of ongoing work. As illustrated by the Fourier transform infrared spectroscopy (FTIR) spectra in Figure S7, the absence of TMAOH peaks in the flocs indicates that TMA⁺ is fully displaced during ion exchange. The reduction in width and intensity in the O-H stretching (3,060–3,650 cm⁻¹) mode, on the other hand, suggests that we have proton displacement as well.

In addition to quantifying the dissolved organics as a result of the dye degradation process, we noticed an increase in COD between the starting dye concentration and post-adsorption equilibrium (Figure S5). The measured COD for the initial starting dye was 30 mg/L for both dyes; after adsorption, it spiked to 110 mg/L for CV and 90 mg/L for Rh6G. The observed spike can be attributed to the release of TMA $^+$ or (CH $_3$) $_4$ N $^+$ cations, which are organic and would be oxidized by the dichromate during COD analysis.

The as-synthesized 1DL structure is outlined in Figure 2C, where the a,b, and c parameters are $3.0\,\text{Å}$, $11.5\,\text{Å}$, and $3.7\,\text{Å}$, respectively, consistent with the XRD pattern in Figure 2A. When the dye is added to the system, it replaces the TMA⁺, as evidenced by a large shift in d-spacing (Figure 6F). The d-spacings with Rh6G and CV are $22.1\,\text{Å}$ and $20.8\,\text{Å}$, respectively. In both cases, there is still stacking in the (0k0) direction. Given the dimensions of the former, to account for this spacing, it is reasonable to assume that there is a preferential stacking orientation, as shown in Figure 9A. This behavior has been simulated in MMT clays and is indicative of an increase in d-spacing between the clay layers by $\sim 10\,\text{Å}$, consistent with the increase we see. In the CV case, stacking may be related to an orientation that maximizes π - π interactions between the pendant groups of the CV, as illustrated in Figure 9B. These comments notwithstanding, much more work, some of it theoretical, is needed before the dye configurations shown in Figure 9 are confirmed. Some of this work is ongoing but out of the scope of this paper.

The most important result of this work is the strong evidence that the 1DLs are sensitized by both dyes. This is best seen in Figures 7C and 7D; without sensitization, a



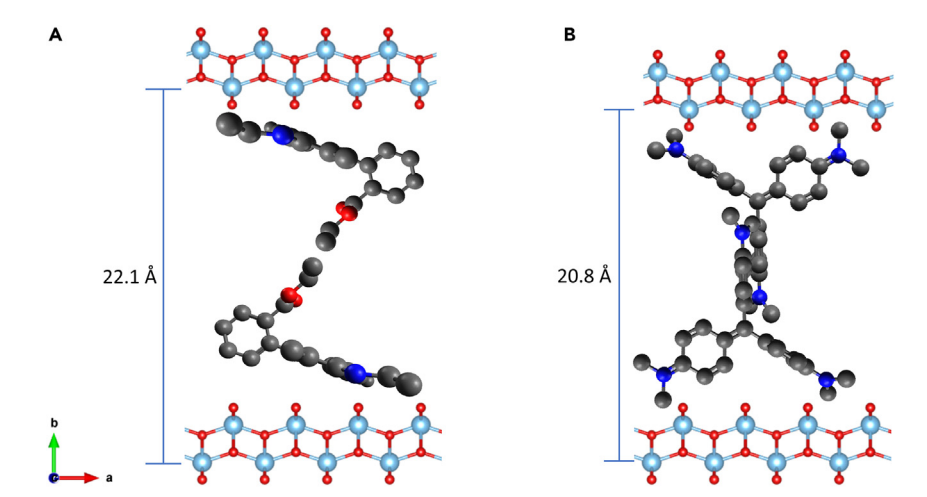


Figure 9. Schematics of 1DLs with dve intercalants Proposed adsorption modes for (A) Rh6G and (B) CV. Interplanar spacings were obtained from XRD patterns shown in Figure 6F. Schematics are to scale.

material with an $E_{\rm q}$ of greater than 3.0 eV should not degrade dyes solely in the visible spectrum. This is why P25 is practically inert in the visible spectrum (top, horizontal, solid lines in Figures 7C and 7D). To ensure that bleaching was not contributing to decolorization, the dyes alone were illuminated in the experimental setup. On the timescale of 30 min, under 1-sun irradiance, the dyes exhibited essentially no bleaching (Figure S9). The fact that our 1DLs are quite active in the visible spectrum thus has to be due to dye sensitization.

Sensitization hinges significantly on the contact between the semiconductor and the sensitizing dye.⁵⁰ There is a noteworthy amount of work regarding TiO₂, especially P25, on improving its ability to adsorb a sensitizing dye onto its surface. In a pair of studies, when P25 was placed in water for various amounts of time before adding it to the dye system, ^{27,31} its surface became more active vis-à-vis adsorption. This was attributed to the localized positive and negative charges supplied by the adsorbed water and deprotonated hydroxyls, respectively.^{27,31} Because 1DLs vastly outperform P25 in terms of dye adsorption, especially with respect to surface charge, it is reasonable to conclude that this is a main driver in enabling sensitization behavior.

Adsorption is not the only key to self-sensitization. To support our self-sensitization conjecture, we plotted the oxidation potentials of 1DLs⁴² alongside those of each dye in Figure 10. In both cases, it is clear that, upon exposure to light, an electron in the dye's excited state can inject into the CB of the 1DLs. When free electrons are available in the CB, they can readily react with dissolved O2, forming O2. radicals, which, in turn, form other ROS.³² This electron transfer to the CB is necessary because of the poor kinetics of electron transfer between dissolved O_2 and an excited dye molecule.⁵¹ Excited-state electronic properties of CV and Rh6G are available in the literature. 52,53 The differences in their excited and ground states were calculated using the photon energies of their associated excitation wavelengths, 2.10 eV and 2.36 eV, respectively.

Sensitization of TiO₂ particles is quite well studied in the literature, primarily for use in solar cells. Rhodamines, including Rh6G, and CV were used in multiple studies for the sensitization of nano-TiO₂. ^{10,18,27,28,54} Self-sensitization of P25 has been studied for rhodamine B³² but, to the best of our knowledge, not CV. In the former case, the



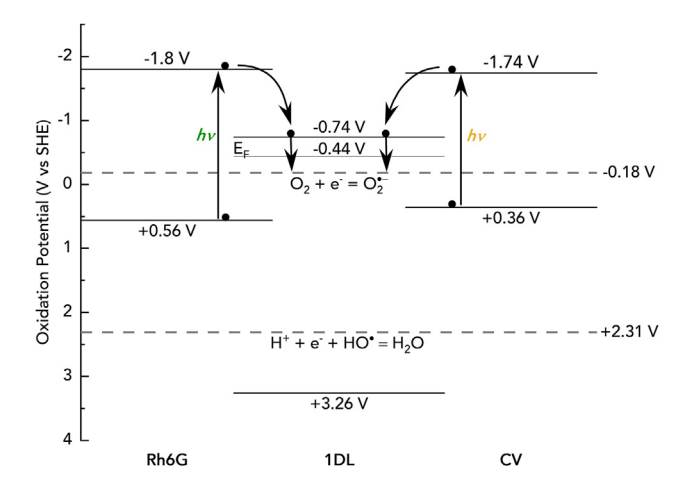


Figure 10. Oxidation potential diagram vs. standard hydrogen electrode (SHE), showing electronic structures of Rh6G, 1DL, and CV

Left: electronic structure of Rh6G. Center: electronic structure of 1DL. Right: electronic structure of CV. Electronic properties of 1DL were reproduced from Colin-Ulloa et al. 42 Excited-state values for CV and Rh6G were taken from Islam et al. 52 and Ghosh and König, 53 respectively. Also plotted are the potentials for the formation of O_2 and O_2 and O_2 are similar proposed electron flow via the sensitization mechanism.

dyes degrade via dealkylation mechanisms.²³ There is no reason to surmise that the situation is not the same here. This conclusion is supported by the hypsochromic shifts plotted in Figures 7A and 7B that are consistent with those in the literature.^{27,30,32}

The importance of this self-sensitization behavior in a first-generation material cannot be overstated. In most published studies, the ${\rm TiO_2}$ must be illuminated for hours, sometimes at low pH, to see any quantifiable decolorization. 32,33 2D titanates do not exhibit the level of visible light activity we demonstrate here, even with the inclusion of precious metals like gold and palladium 55 or functionalization with peroxo-titanium complexes. 56 To the best of our knowledge, the only study with comparable self-sensitization behavior (>90% decolorization of rhodamine B in \approx 20 min) does not use ${\rm TiO_2}$ as an electron mediator. Periodate (${\rm IO_4}^-$) was utilized as the electron mediator by an experimental method similar to ours but with a visible light intensity of more than 2.5 suns compared with 1 sun used here. During the reaction, ${\rm IO_4}^-$ is reduced to ${\rm IO_3}^-$, while the dye is oxidized and ultimately decolorized. 57 Importantly, with a homogeneous catalyst system, such as the periodate system, the ability to adsorb any dye is completely removed. In our case, the kinetics of dye degradation are significant, but that is after the 1DLs adsorb nearly 60% of the dye in solution before light hits the sample.

Conclusions

Rh6G and CV are degraded by a highly adsorbent one-dimensional titanium oxide-based colloidal catalyst in neutral aqueous dispersions under a simulated solar spectrum. These materials exhibit essentially instantaneous adsorption with exceptional uptake capacity for Rh6G and CV, at 1,850 mmol kg $^{-1}$ and 1,930 mmol kg $^{-1}$, respectively – more than twice that of highly adsorbent MMT clay. Under a full spectrum, the colloidal catalyst outperforms P25 in decolorizing Rh6G, with PFO rate constants of 0.12 min $^{-1}$ and 3.1 x 10^{-2} min $^{-1}$, respectively, while for CV they performed equally, with a rate constant \approx 3.1 x 10^{-2} min $^{-1}$. Under visible light alone, these



materials decolorize both CV and Rh6G by at least 60% in 30 min. Under comparable conditions P25 is inactive.

As a 1D photocatalyst, the material in this study demonstrates a highly negative surface and available surface area working in conjunction with the ability of common waste dyes to absorb light in the visible spectral range. These materials demonstrate exceptional potential to be sensitized by said dyes. The implications of these discoveries for other areas like solar cells, chemical production, and further pollutant degradation is abundantly clear. We hope this work sparks further development in these spaces.

EXPERIMENTAL PROCEDURES

Resource availability

Lead contact

Further requests regarding resources and/or reagents should be directed to the lead contact, Michel W. Barsoum (barsoumw@drexel.edu).

Materials availability

This study did not generate new reagents.

Data and code availability

Data, pre or post processed, presented in this study are available upon request from the lead contact.

Materials

The materials utilized in this study were TiB₂ (as received, 99.9%, 325 mesh; Thermo Fisher Scientific, Waltham, MA, USA), TiN (as received, 99.7%, <4 μ m, Thermo Fisher Scientific), TiC (as received, 99.5%, 2 μ m, Thermo Fisher Scientific), TMAOH (as received, 25% [w/w] aqueous 99.9999%; Alfa Aesar, Ward Hill, MA, USA), ethanol (200 proof; Decon Laboratories, King of Prussia, PA, USA), Aeroxide P25 (as received, Thermo Fisher Scientific), MMT-benton (as received; Avantor, Radnor, PA, USA), Rh6G (as received, 99%, Thermo Fisher Scientific), CV (as received, lab grade; Ward's Science+, ON, Canada), and NaCl (as received, 99%; Thermo Fisher Scientific). Ultrapure dionized water (DI), <18.2 m Ω /cm, was utilized for all methods outlined below.

Synthesis of 1DLs

Precursor powders (TiB_2 , TiN, and TiC) were immersed in TMAOH in 250 mL polyethylene bottles that were heated and shaken in an incubator (shaking incubator; Labnet International, NJ, USA) at 200 rpm and 80° C for 3 days. Each bottle was vented with a single 23G needle. The weights of each reactant were chosen to keep a Ti:TMAOH molar ratio of 0.6:1, which is the ratio we have been working with since the discovery of these 1DLs. This is by no means the optimal ratio with respect to reaction kinetics, but it was used here so we can compare the results in this work with previous and ongoing, work. Each 1DL synthesis starts with 10 g of precursor, and based on the 0.6:1 molar ratio, the mass of 25% (w/w) TMAOH solution varies. The powders formed when the precursors were TiB_2 , TiN, and TiC are referred in this study as 1DL, C-1DL, and N-1DL, respectively. For 1DL, formed from the highest-molecular-weight precursor, only 87.5 g of TMAOH solution is required. The lower-molecular-weight precursors, C-1DL and N-1DL, required 100 g and 98 g of TMAOH, respectively.

After the reaction, the resulting sediment was combined with ethanol, vortex shaken, and centrifuged several times at 3,500 rpm for 2 min until a clear supernatant





and neutral pH were achieved (usually 3 times). Water was added to the ethanol-washed product, and the material was suspended by vortex shaking. After centrifugation, a highly stable colloidal suspension was obtained while unreacted powders settled to the bottom. The colloidal 1DLs were each diluted to an initial known concentration determined by vacuum filtering 2 mL of colloidal 1DL through a 25- μ m-thick microporous monolayer polypropylene membrane (Celgard 3501; Celgard, NC, USA) over a fritted glass filter apparatus. After filtering, the solid was fully dried in an oven, under a mechanical vacuum, at 80°C, and the weight of the residue was measured.

Material characterization

Filtered films were prepared by the filtering method detailed in Synthesis of 1DLs. When flocs were utilized for analysis, they were washed 3 times with DI water and filtered to remove the water. The morphologies of the flocs were imaged using a field emission SEM (Supra 50VP; Carl Zeiss, Jena, Germany). Because of the nonconducting nature of our samples, they were sputtered for 30 s at 40 mV with a Pt/Pd sputter coater (208HR; Cressington Scientific Instruments, Watford, UK). Drop-cast colloids were imaged using a field emission transmission electron microscope (JEM-F200; JEOL, Tokyo, Japan). The crystal structure of the finely crushed filtered films and flocs were analyzed using an X-ray diffractometer (MiniFlex; Rigaku, Tokyo, Japan) with a step of 0.02° and a 1-s hold time with Cuk_{α} radiation at 40 kV.

The light absorption behavior of the 1DL colloid, diluted to 10 mg/L, was recorded using an UV-visible (UV-vis) spectrophotometer (Cary 60; Agilent Technologies, CA, USA) with a scan rate of 60 nm/min. The scan was taken through a quartz cuvette with a 1-cm path length. The optical band gap was obtained using the Tauc method as outlined by Makuła et al. 58

Monitoring the dye decolorization process

Dye concentrations were determined using the UV-vis spectrophotometer at a scan rate of 300 nm/min. As shown in Figure S8, the λ_{max} for Rh6G and CV was 526 nm and 590 nm, respectively. Spectra were obtained across the visible light range and into the UV range to monitor peak intensity reductions, peak shifts, and/or formation of new peaks. Polymethyl methacrylate (PMMA) cuvettes with a 1-cm path length were used for measurements in the 800–300 nm range. Quartz cuvettes were used in the 300 nm range or less. The UV-vis calibration curve, or Beer-Lambert plots, are available in Figure S8, along with the derivation of the Beer-Lambert relationship shown in Scheme S1. Dye samples were diluted as necessary to get within the linear portion of the Beer-Lambert plot and re-scaled to get bulk concentrations.

Adsorption of Rh6G and CV on 1DLs

Stock aqueous suspensions of 1DL and MMT were mixed to a concentration of 1 g/L. Assuming that the active unit of 1DL is TiO_2 , by disregarding surface terminations and the displaced TMA^+ , the concentration of 1DL in the colloidal suspension is 12.5 mM. MMT is a semi-stable colloid at neutral pH, allowing easy resuspension upon separating out. Stock aqueous solutions of Rh6G and CV with concentrations of 0.5 g/L (1.0 mM and 1.2 mM, respectively) were also prepared and used in all tests here.

To ensure good dye/catalyst/adsorbent mixing, each mixture was placed in a 20-mL polyethylene terephthalate (PET) vial in an enclosed container strapped to an orbital shaker. The container was a hollowed-out Styrofoam box with a tight-fitting lid—to



prevent light from entering—that held the vials stationary while the container was attached to the orbital shaker, which was shaken at a constant rate of 200 rpm.

In the kinetics of adsorption experiments, the vials were each loaded with 0.5 mL of stock 1DL colloid and 8.5 mL DI and lightly hand shaken. 1 mL of the stock dye solution was then added. The vial was placed in the container and allowed to shake at 200 rpm. At specified time intervals, the vials were removed, and the mixture was filtered through a 0.45- μ m polytetrafluoroethylene (PTFE) syringe filter to remove any suspended solids. In some situations, the resulting solution was diluted with water to lower its concentration for UV-vis analysis.

To determine the room-temperature adsorption isotherm, 1DL and MMT colloids were prepared according to details listed in Table S8. The samples were allowed to shake for 1 h to ensure that equilibrium was reached. After 1 h, the mixture was again filtered through a $0.45-\mu m$ PTFE syringe filter.

Impact of ionic strength of solution on adsorption of Rh6G

A 5 M solution of NaCl was prepared. The same adsorption orbital shaker setup was utilized for this experiment (see Adsorption of Rh6G and CV on 1DLs.). The vials were each loaded with 0.5 mL of the stock 1DL colloid and 3.5 mL DI and lightly hand shaken. 1 mL of stock dye solution was then added, and the vials were shaken for 30 min at 200 rpm. NaCl solutions were added to each vial as outlined in Table S9. The new mixtures were allowed to shake for an additional 30 min, and the mixture was then filtered through 0.45- μ m PTFE syringe filter.

Full-solar-spectrum photocatalytic decolorization of Rh6G and CV

A stock aqueous suspension of P25 was mixed to a concentration of 1 g/L (12.5 mM). P25 forms a semi-stable colloid at neutral pH, allowing easy resuspension upon separating out. Note that the stock P25 solution was allowed to sit in water prior to its use in any experiment to ensure full hydration. The work of Pan et al.²⁷ showed improved capability for P25 to exhibit self-sensitization behavior when hydrated. However, when P25 remains in water for >7 days, it clumps and loses much of its activity.^{27,31} Whenever a 1DL colloid was made, we suspended the P25 used in this study in water. This kept the two systems at an equal level of hydration for even comparison.

The experimental setup included an artificial sun, which consisted of a 300-W xenon (Xe) lamp (MAX 350 with UV-vis mirror module, quartz light guide, and ×1.0 type collimator; Asahi Spectra, Tokyo, Japan), positioned directly above a stir plate. The lamp's spectrum used in this study is reproduced in Figure \$10. Before each run, the lamp's output irradiance was measured using a thermal power meter (\$401C thermal power sensor head with a PM400 console; Thorlabs, Newton, NJ, USA). In an effort to maintain consistency, an irradiance of 100 mW/cm², equivalent to 1 sun, was obtained and used throughout by changing the distance between the collimator and the surface of the dye/catalyst system. The aqueous dye and catalyst mixture was placed in a 20-mL beaker (~2-cm inner diameter) and constantly stirred at 400 rpm with a 10-mm PTFE-coated magnetic stir bar. To prevent stray light, the beaker was wrapped in opaque tape.

Overall, the experimental process was straightforward and designed to control the amount of catalyst to dye by mass for each run. For the 10:1 mass ratio, 17.6 mL of water was added to the beaker, followed by 2 mL of stock colloidal catalyst. This mixture was allowed to stir for a few seconds prior to introducing 0.4 mL of stock





dye. For the 1:1 mass ratio, 19.4 mL of water was added to a beaker, followed by 0.2 mL of stock colloidal catalyst and then 0.4 mL of stock dye solution. This dye concentration was used because it fell within the linear region of the Beer-Lambert plot for the dyes, which prevents the need for dilution that can reduce impact of dye/dye interactions. When the dye and catalyst were mixed, the beaker was covered with an opaque lid and left to stir for 30 min to achieve an adsorption equilibrium. After 30 min in the dark, the lid was removed, and the lamp was turned on. After a predefined time, a 2-mL aliquot was taken from the main batch and filtered through a 0.45- μ m PTFE syringe filter to filter out any catalyst and isolate the solution. If the dye and material formed a complex, as with the 10:1 mass ratio, it was vacuum filtered through Celgard.

Partial-spectrum photocatalytic decolorization of Rh6G and CV

To measure dye decolorization under UV and vis illumination separately, the same experimental setup was used as for the 1:1 mass ratio full-spectrum decolorization experiments (see Full-solar-spectrum photocatalytic decolorization of Rh6G and CV). Optical filters—400-nm short pass (model 84-702) and 400-nm long pass (model 62-981) (OD 4.0; Edmund Optics, Barrington, NJ, USA)—were employed to remove the vis and UV portions of the Xe spectrum, respectively. Because the filters inherently block about 9% of transmitted light, a total UV-vis irradiance of 110 mW/cm² was used by changing the distance between the collimator and the surface of the dye/catalyst system before the filters were placed in the light path. The sampling method employed was the same as for the full-spectrum tests.

Quantifying mineralization: COD of dye samples

Degradation was confirmed via low-range (LR) COD using the dichromate reactor digestion method, a United States Environmental Protection Agency accepted wastewater analysis technique (K-7355; CHEMetrics, Midland, VA, USA). The manufacturer-supplied calibration equation, $C = -331[Abs_{sample} - Abs_{Dl}] - 0.6$, was used in our study to determine concentration of dissolved organics in the solutions. This equation relates the concentration of dissolved organics, C, in mg/L, to the relative absorbance of the resulting solution after digestion in the COD vial. Abs denotes the light absorption value at 420 nm. To increase the concentration of organics into the center of the LR COD kit, the same 1:1 catalyst-to-dye mass ratio was kept but 5 times scaled. First, 17 mL of DI was added to the same setup as in Full-solar-spectrum photocatalytic decolorization of Rh6G and CV, followed by 1 mL of stock colloidal 1DL and then 2 mL of dye. The sampling procedure was the same as for the full-spectrum tests. Here, dye samples needed to be diluted into the linear range of the Beer-Lambert plot before being placed in the UV-vis spectrophotometer.

SUPPLEMENTAL INFORMATION

Supplemental information can be found online at https://doi.org/10.1016/j.matt. 2023.09.008.

ACKNOWLEDGMENTS

XRD and SEM analyses were completed in the Materials Characterization Core at Drexel University. We would like to thank Dr. Yong-Jie Hu of Drexel University's Department of Materials Science and Engineering for supplying the calculated 1DL structure. We would also like to thank Dr. Charles W. Ross III, Director Automated Synthesis and Characterization, Center Director MS, BCRC, HTE-Analytical of the University of Pennsylvania Chemistry Department for providing chromatographic/mass spectral method development, analyses, and data interpretation.



We also want to note that Figure 1 was partially created with BioRender.com. This work was funded by the Ceramics Program of the National Science Foundation Division of Materials Research (DMR-2211319).

AUTHOR CONTRIBUTIONS

Conceptualization, A.D.W., J.C., and M.W.B.; methodology, A.D.W. and G.R.S.; validation, A.D.W., G.R.S., and A.J.L.; formal analysis, A.D.W.; investigation, A.D.W., G.R.S., K.S., M.Q.H., L.F., and A.M.; resources, M.W.B.; writing – original draft, A.D.W.; writing – review & editing, G.R.S., A.J.L., and M.W.B.; supervision, M.W.B.; funding acquisition, M.W.B.

DECLARATION OF INTERESTS

One of the authors, M.W.B., filed for a patent on the 1D TiO_2 , which is the subject of this work.

Received: July 17, 2023 Revised: August 31, 2023 Accepted: September 18, 2023 Published: October 10, 2023

REFERENCES

- Mani, S., and Bharagava, R.N. (2016). Exposure to Crystal Violet, Its Toxic, Genotoxic and Carcinogenic Effects on Environment and Its Degradation and Detoxification for Environmental Safety. Rev. Environ. Contam. Toxicol. 237, 71–104. https://doi.org/10.1007/ 978-3-319-23573-8_4.
- Gessner, T., and Mayer, U. (2000). Triarylmethane and Diarylmethane Dyes. Ullmann's Encyclopedia of Industrial Chemistry. https://doi.org/10.1002/14356007. a27_179.
- Rasheed, T., Bilal, M., Iqbal, H.M.N., Hu, H., and Zhang, X. (2017). Reaction Mechanism and Degradation Pathway of Rhodamine 6G by Photocatalytic Treatment. Water Air Soil Pollut. 228, 291. https://doi.org/10.1007/s11270-017-3458-6.
- Thaler, S., Haritoglou, C., Choragiewicz, T.J., Messias, A., Baryluk, A., May, C.A., Rejdak, R., Fiedorowicz, M., Zrenner, E., and Schuettauf, F. (2008). In Vivo Toxicity Study of Rhodamine 6G in the Rat Retina. Invest. Ophthalmol. Vis. Sci. 49, 2120–2126. https://doi.org/10.1167/iovs. 07-1476.
- Grauer, Z., Avnir, D., and Yariv, S. (1984). Adsorption characteristics of rhodamine 6G on montmorillonite and laponite, elucidated from electronic absorption and emission spectra. Can. J. Chem. 62, 1889–1894. https://doi.org/ 10.1139/w84-324
- Li, Z., Potter, N., Rasmussen, J., Weng, J., and Lv, G. (2018). Removal of rhodamine 6G with different types of clay minerals. Chemosphere 202, 127–135. https://doi.org/10.1016/j. chemosphere.2018.03.071.
- Annadurai, G., Juang, R.S., and Lee, D.J. (2001). Adsorption of Rhodamine 6G from aqueous solutions on activated carbon. J. Environ. Sci. Health. A Tox. Hazard. Subst. Environ. Eng. 36,

- 715–725. https://doi.org/10.1081/ESE-100103755.
- Phoemphoonthanyakit, S., Seeharaj, P., Damrongsak, P., and Locharoenrat, K. (2019). Effect of Adsorption Characteristics of Rhodamine 6G Dye Solution in Fe₃O₄ Magnetic Nanoparticles on Fluorescence Quantum Yield. Journal of Spectroscopy 2019, 1–5. https://doi.org/10.1155/2019/2853989.
- Shen, K., and Gondal, M.A. (2017). Removal of hazardous Rhodamine dye from water by adsorption onto exhausted coffee ground.
 J. Saudi Chem. Soc. 21, 5120–5127. https://doi. org/10.1016/j.jscs.2013.11.005.
- Aduroja, O., Jani, M., Ghann, W., Ahmed, S., Uddin, J., and Abebe, F. (2022). Synthesis, Characterization, and Studies on Photophysical Properties of Rhodamine Derivatives and Metal Complexes in Dye-Sensitized Solar Cells. ACS Omega 7, 14611–14621. https://doi.org/10. 1021/acsomega.1c06772.
- Lee, S.Y., Kang, D., Jeong, S., Do, H.T., and Kim, J.H. (2020). Photocatalytic Degradation of Rhodamine B Dye by TiO₂ and Gold Nanoparticles Supported on a Floating Porous Polydimethylsiloxane Sponge under Ultraviolet and Visible Light Irradiation. ACS Omega 5, 4233–4241. https://doi.org/10.1021/ acsomega.9b04127.
- Sanakousar, M.F., Cc, V., Jiménez-Pérez, V., Jayanna, B., Jayanna, B.K., Shridhar, A., and Prakash, K. (2021). Efficient photocatalytic degradation of crystal violet dye and electrochemical performance of modified MWCNTs/Cd-ZnO nanoparticles with quantum chemical calculations. J. Hazard. Mater. Adv. 2, 100004. https://doi.org/10.1016/ j.hazadv.2021.100004.
- Xiang, Q., Yu, J., and Wong, P.K. (2011). Quantitative characterization of hydroxyl radicals produced by various photocatalysts.

- J. Colloid Interface Sci. 357, 163–167. https://doi.org/10.1016/j.jcis.2011.01.093.
- Ohtani, B., Prieto-Mahaney, O.O., Li, D., and Abe, R. (2010). What is Degussa (Evonik) P25? Crystalline composition analysis, reconstruction from isolated pure particles and photocatalytic activity test. J. Photochem. Photobiol. Chem. 216, 179–182. https://doi. org/10.1016/j.jphotochem.2010.07.024.
- Tobaldi, D.M., Pullar, R.C., Seabra, M.P., and Labrincha, J.A. (2014). Fully quantitative X-ray characterisation of Evonik Aeroxide TiO₂ P25. Mater. Lett. 122, 345–347. https://doi.org/10. 1016/j.matlet.2014.02.055.
- Lee, S.-Y., and Park, S.-J. (2013). TiO₂
 photocatalyst for water treatment applications.
 J. Ind. Eng. Chem. 19, 1761–1769. https://doi.org/10.1016/j.jiec.2013.07.012.
- Fujishima, A., Zhang, X., and Tryk, D. (2008). TiO₂ photocatalysis and related surface phenomena. Surf. Sci. Rep. 63, 515–582. https://doi.org/10.1016/j.surfrep.2008.10.001.
- Pino, E., Calderón, C., Herrera, F., Cifuentes, G., and Arteaga, G. (2020). Photocatalytic Degradation of Aqueous Rhodamine 6G Using Supported TiO₂ Catalysts. A Model for the Removal of Organic Contaminants From Aqueous Samples. Front. Chem. 8, 365. https:// doi.org/10.3389/fchem.2020.00365.
- Sangchay, W., Sikong, L., and Kooptarnond, K. (2012). Comparison of photocatalytic reaction of commercial P25 and synthetic TiO₂-AgCI nanoparticles. Procedia Eng. 32, 590–596. https://doi.org/10.1016/j.proeng.2012. 01.1313.
- 20. Wang, Z., Xu, J., Li, Y., Wang, K., Wang, Y., Hong, Q., Li, W.J., and Li, S.P. (2010). Study on the shape control and photocatalytic activity of high-energy anatase titania. Int. J. Syst. Evol.





- Microbiol. 60, 378–381. https://doi.org/10.1016/j.apcatb.2010.08.014.
- Chen, F., Fang, P., Gao, Y., Liu, Z., Liu, Y., and Dai, Y. (2012). Effective removal of high-chroma crystal violet over TiO₂-based nanosheet by adsorption–photocatalytic degradation. Chem. Eng. J. 204–206, 107–113. https://doi. org/10.1016/j.cej.2012.07.030.
- Lachheb, H., Puzenat, E., Houas, A., Ksibi, M., Elaloui, E., Guillard, C., and Herrmann, J.-M. (2002). Photocatalytic degradation of various types of dyes (Alizarin S, Crocein Orange G, Methyl Red, Congo Red, Methylene Blue) in water by UV-irradiated titania. Appl. Catal. 39, 75–90. https://doi.org/10.1016/S0926-3373(02) 00078-4.
- Chiu, Y.-H., Chang, T.-F., Chen, C.-Y., Sone, M., and Hsu, Y.-J. (2019). Mechanistic Insights into Photodegradation of Organic Dyes Using Heterostructure Photocatalysts. Catalysts 9, 430. https://doi.org/10.3390/catal9050430.
- Kumar, S.G., and Devi, L.G. (2011). Review on Modified TiO₂ Photocatalysis under UV/Visible Light: Selected Results and Related Mechanisms on Interfacial Charge Carrier Transfer Dynamics. J. Phys. Chem. A 115, 13211–13241. https://doi.org/10.1021/ jp204364a.
- Nosaka, Y., and Nosaka, A. (2016). Understanding Hydroxyl Radical (OH) Generation Processes in Photocatalysis. ACS Energy Lett. 1, 356–359. https://doi.org/10. 1021/acsenergylett.6b00174.
- Zhang, J., and Nosaka, Y. (2013). Quantitative Detection of OH Radicals for Investigating the Reaction Mechanism of Various Visible-Light TiO₂ Photocatalysts in Aqueous Suspension. J. Phys. Chem. C 117, 1383–1391. https://doi.org/ 10.1021/jp3105166.
- Pan, L., Zou, J.-J., Zhang, X., and Wang, L. (2011). Water-Mediated Promotion of Dye Sensitization of TiO₂ under Visible Light. J. Am. Chem. Soc. 133, 10000–10002. https://doi.org/10.1021/ja2035927.
- Qurratulain, Hameed, S., Kazmi, S.A., Ahmad, N., Khan, W. (2015). Effect of Different Dyes on TiO₂ Based Dye Sensitized Solar Cell, 17–20; p. 1–6. https://doi.org/10.1109/indicon.2015. 7443767.
- Hagfeldt, A., Boschloo, G., Sun, L., Kloo, L., and Pettersson, H. (2010). Dye-Sensitized Solar Cells. Chem. Rev. 110, 6595–6663. https://doi. org/10.1021/cr900356p.
- Cassidy, J.P., Tan, J.A., and Wustholz, K.L. (2017). Probing the Aggregation and Photodegradation of Rhodamine Dyes on TiO₂. J. Phys. Chem. C 121, 15610–15618. https://doi.org/10.1021/acs.jpcc.7b04604.
- Pan, L., Zou, J.-J., Liu, X.-Y., Liu, X.-J., Wang, S., Zhang, X., and Wang, L. (2012). Visible–Light– Induced Photodegradation of Rhodamine B over Hierarchical TiO₂: Effects of Storage Period and Water-Mediated Adsorption Switch. Ind. Eng. Chem. Res. 51, 12782–12786. https://doi.org/10.1021/ie3019033.
- 32. Wu, T., Liu, G., Zhao, J., Hidaka, H., and Serpone, N. (1998). Photoassisted Degradation of Dye Pollutants. V. Self-Photosensitized Oxidative Transformation of Rhodamine B under Visible Light Irradiation in Aqueous TiO₂

- Dispersions. J. Phys. Chem. B *102*, 5845–5851. https://doi.org/10.1021/jp980922c.
- Zhang, F., Zhao, J., Shen, T., Hidaka, H., Pelizzetti, E., and Serpone, N. (1998). TiO₂assisted photodegradation of dye pollutants II. Adsorption and degradation kinetics of eosin in TiO₂ dispersions under visible light irradiation. Appl. Catal. B Environ. 15, 147–156. https://doi.org/10.1016/S0926-3373(97) 00043-X.
- Kolen'ko, Y.V., Kovnir, K.A., Gavrilov, A.I., Garshev, A.V., Frantti, J., Lebedev, O.I., Churagulov, B.R., Van Tendeloo, G., and Yoshimura, M. (2006). Hydrothermal Synthesis and Characterization of Nanorods of Various Titanates and Titanium Dioxide. J. Phys. Chem. B 110, 4030–4038. https://doi.org/10.1021/ jp055687u.
- 35. Yin, H., Ding, G., Gao, B., Huang, F., Xie, X., and Jiang, M. (2012). Synthesis of ultrafine titanium dioxide nanowires using hydrothermal method. Mater. Res. Bull. 47, 3124–3128. https://doi.org/10.1016/j.materresbull.2012.08.022
- 36. Ge, M., Cao, C., Huang, J., Li, S., Chen, Z., Zhang, K.-Q., Al-Deyab, S.S., and Lai, Y. (2016). A review of one-dimensional TiO₂ nanostructured materials for environmental and energy applications. J. Mater. Chem. A Mater. 4, 6772–6801. https://doi.org/10.1039/ c5ta09323f.
- Weng, B., Liu, S., Tang, Z.-R., and Xu, Y.-J. (2014). One-dimensional nanostructure based materials for versatile photocatalytic applications. RSC Adv. 4, 12685–12700. https:// doi.org/10.1039/C3RA47910B.
- Badr, H.O., El-Melegy, T., Carey, M., Natu, V., Hassig, M.Q., Johnson, C., Qian, Q., Li, C.Y., Kushnir, K., Colin-Ulloa, E., et al. (2022). Bottom-up, scalable synthesis of anatase nanofilament-based two-dimensional titanium carbo-oxide flakes. Mater. Today 54, 8–17. https://doi.org/10.1016/j.mattod.2021.10.033.
- Badr, H.O., Lagunas, F., Autrey, D.E., Cope, J., Kono, T., Torita, T., Klie, R.F., Hu, Y.-J., and Barsoum, M.W. (2023). On the structure of onedimensional TiO₂ lepidocrocite. Matter 6, 128–141. https://doi.org/10.1016/j.matt.2022. 10.015.
- Badr, H.O., Cope, J., Kono, T., Torito, T., Lagunas, F., Castiel, E., Klie, R.F., and Barsoum, M.W. (2023). Titanium Oxide-based 1D Nanofilaments, 2D Sheets, and Mesoporous Particles - Synthesis, Characterization and Ion Intercalation. Matter. https://doi.org/10.1016/j. matt.2023.07.022.
- Wang, L., Badr, H.O., Yang, Y., Cope, J.H., Ma, E., Ouyang, J., Yuan, L., Li, Z., Liu, Z., Barsoum, M.W., and Shi, W. (2023). Unique hierarchical structures of one dimensional lepidocrocite titanate with cation-exchangeable sites for extraordinary selective actinide capture for water purification. Chem. Eng. J. 474, 145635. https://doi.org/10.1016/j.cej.2023.145635.
- Colin-Ulloa, E., Martin, J.L., Hanna, R.J., Frasch, M.H., Ramthun, R.R., Badr, H.O., Uzarski, J.R., Barsoum, M.W., Grimm, R.L., and Titova, L.V. (2023). Electronic Structure of 1D Lepidocrocite TiO₂ as Revealed by Optical Absorption and Photoelectron Spectroscopy. J. Phys. Chem. C

- 127, 7275–7283. https://doi.org/10.1021/acs.jpcc.2c06719.
- 43. Liao, T., Sun, Z., and Dou, S.X. (2017). Theoretically Manipulating Quantum Dots on Two-Dimensional TiO₂ Monolayer for Effective Visible Light Absorption. ACS Appl. Mater. Interfaces 9, 8255–8262. https://doi.org/10. 1021/acsami.6b15741.
- Sasaki, T., Watanabe, M., Michiue, Y., Komatsu, Y., Izumi, F., and Takenouchi, S. (1995). Preparation and Acid-Base Properties of a Protonated Titanate with the Lepidocrocitelike Layer Structure. Chem. Mater. 7, 1001– 1007. https://doi.org/10.1021/cm00053a029.
- Hou, C., Hu, B., and Zhu, J. (2018). Photocatalytic Degradation of Methylene Blue over TiO₂ Pretreated with Varying Concentrations of NaOH. Catalysts 8, 575. https://doi.org/10.3390/catal8120575.
- Habib, M.A., Muslim, M., Shahadat, M.T., Islam, M.N., Ismail, I.M.I., Islam, T.S.A., and Mahmood, A.J. (2013). Photocatalytic decolorization of crystal violet in aqueous nano-ZnO suspension under visible light irradiation. J. Nanostructure Chem. 3, 70. https://doi.org/10.1186/2193-8865-3-70.
- Guz, L., Curutchet, G., Torres Sánchez, R., and Candal, R. (2014). Adsorption of crystal violet on montmorillonite (or iron modified montmorillonite) followed by degradation through Fenton or photo-Fenton type reactions. J. Environ. Chem. Eng. 2, 2344– 2351. https://doi.org/10.1016/j.jece.2014. 02.007.
- 48. Abdullah, P.S., Wen, L.K., Awang, H., and Mohammad Azmin, S.N.H. (2021). Rhodamine 6G Removal from Aqueous Solution with Coconut Shell-Derived Nanomagnetic Adsorbent Composite (Cs-Nmac): Isotherm and Kinetic Studies. Pertanika Journal of Science and Technology 29, 1535–1556.
- Sattar, M. (2010). Adsorption of Crystal Violet on Commercial Activated Carbon and Activated Carbon Obtained from Bagasse (Master of Science (Prince of Songkla University).
- Kalyanasundaram, K., and Grätzel, M. (1998). Applications of functionalized transition metal complexes in photonic and optoelectronic devices. Coord. Chem. Rev. 177, 347–414. https://doi.org/10.1016/S0010-8545(98) 00189-1.
- Kyung, H., Lee, J., and Choi, W. (2005). Simultaneous and Synergistic Conversion of Dyes and Heavy Metal Ions in Aqueous TiO₂ Suspensions under Visible-Light Illumination. Environ. Sci. Technol. 39, 2376–2382. https:// doi.org/10.1021/es0492788.
- Islam, M.M., Ueno, K., and Misawa, H. (2010). Redox Cycling Effect on the Surface-enhanced Raman Scattering Signal of Crystal Violet Molecules at Nanostructured Interdigitated Array Electrodes. Anal. Sci. 26, 19–24. https:// doi.org/10.2116/analsci.26.19.
- 53. Ghosh, I., and König, B. (2016). Chromoselective Photocatalysis: Controlled Bond Activation through Light-Color Regulation of Redox Potentials. Angew. Chem., Int. Ed. Engl. 55, 7676–7679. https://doi.org/10.1002/anie.201602349.



- Fernando, C.A.N., Kumarawadu, I., Takahashi, K., Kitagawa, A., and Suzuki, M. (1999). Crystal violet dye-sensitized photocurrent by participation of surface states on p-CuSCN photocathode. Sol. Energy Mater. Sol. Cell. 58, 337–347. https://doi.org/10.1016/S0927-0248(99)00006-9.
- Gade, R., Basude, M., Simhachalam, N.B., V, R.D., Pola, S., and Chetti, P. (2022). Synthesis of titanates for photomineralization of industrial wastewater and organic pollutants. Environ. Sci, Water Res. Technol.
- 8, 3065–3078. https://doi.org/10.1039/d2ew00469k.
- 56. Park, H., Goto, T., Cho, S., Nishida, H., and Sekino, T. (2020). Enhancing Visible Light Absorption of Yellow-Colored Peroxo-Titanate Nanotubes Prepared Using Peroxo Titanium Complex Ions. ACS Omega 5, 21753–21761. https://doi.org/10.1021/acsomega.0c02734.
- 57. Yun, E.-T., Yoo, H.-Y., Kim, W., Kim, H.-E., Kang, G., Lee, H., Lee, S., Park, T., Lee, C., Kim, J.-H., and Lee, J. (2017). Visible-light-induced
- activation of periodate that mimics dyesensitization of TiO₂: Simultaneous decolorization of dyes and production of oxidizing radicals. Appl. Catal. B Environ. *203*, 475–484. https://doi.org/10.1016/j.apcatb. 2016.10.029.
- Makuła, P., Pacia, M., and Macyk, W. (2018). How To Correctly Determine the Band Gap Energy of Modified Semiconductor Photocatalysts Based on UV-Vis Spectra. J. Phys. Chem. Lett. 9, 6814–6817. https://doi. org/10.1021/acs.jpclett.8b02892.